Metrol. Meas. Syst., Vol. 32 (2025) No. 1, pp. 1–21
DOI: 10.24425/mms.2025.152775

PAN POLSKA AKADEMIA NAUK

METROLOGY AND MEASUREMENT SYSTEMS
Index 330930, ISSN 0860-8229
www.metrology.wat.edu.pl

M&MS

DETECTION OF STEEL PIPELINE WITHOUT REMOVING CLADDING BASED ON DIFFERENTIAL COMPENSATION PROBE

Xinhua Wang, Zisheng Guo, Tao Sun, Naixiang Hu, Peng Gao, Lin Yang, Ghulam Rasool, Yongsheng Qi

College of Mechanical & Energy Engineering, Beijing University of Technology (✉ *tsun@bjut.edu.cn*)

Abstract

The harmonic magnetic field detection method has the advantage of a large lifting height, which is particularly beneficial for the detection of steel pipelines without removing cladding. However, it has the problem of strong coupling between the excited and induced magnetic field signal, which limits its detection accuracy. In this work, we propose a differential compensation probe, which can effectively suppress the excitation magnetic field signal in the detection signal, in order to significantly improve the accuracy of the harmonic magnetic field detection method. The defect detection capability of the probe is verified both by the finite element simulations and experiments. Despite its simple structure, the differential compensation probe greatly improves the signal-to-noise ratio of the detection signal. It is expected that the detection method based on the differential compensation probe will have a broad application prospect in the detection of pressure pipelines and vessels with cladding layers.

Keywords: steel pipeline, differential compensation probe, cladding layer, defect detection.

1. Introduction

As the key equipment in many important industries such as petroleum, chemical, nuclear power, thermal power, and shipbuilding, pipelines have played an important role in facilitating infrastructure construction and promoting the development of national economies and defence [1]. Various detection methods have been proposed to ensure the safe operation of pipeline transportation, including magnetic flux leakage testing [2], ultrasonic testing [3], pulsed eddy current testing [4,5], digital radiography [6]ayer with a thickness of more than 200 mm to achieve the purpose of thermal insulation, which makes pipeline defect detection [1, 8, 9] very difficult. The harmonic magnetic field detection method, which is used to detect the high-lift steel pipe, is different from the multi-frequency eddy current detection, and its detection signal contains the low-frequency and high-frequency sinusoidal signal at the same time. The low-frequency signals effectively overcome the skin effect of the pipe, and the high-frequency signals are more powerful, thus, the detection signal not only improves the transmission ability of the excitation signal but also improves the

Article history: received May 18, 2024; revised August 10, 2024; accepted October 5, 2024; available online November 19, 2024.

detection sensitivity. [10, 11]. Previously, we designed a harmonic magnetic field detection system including a focused detection probe, which efficiently identified defects outside the pipeline with a 100 mm thick cladding layer [12]. With the increase of the lifting height, the signal-to-noise ratio decays rapidly, which leads to difficulties in obtaining effective information from the detected pipeline. Zhao *et al.* [13] established a finite element model of the magnetic focusing excitation coil, and the simulation results showed that the acquired magnetic field signals were mixed with many noise and interference signals, which hindered the extraction of pipeline defect information. To solve the problem of harmonic signal extraction, Zhao *et al.* [10] designed an orthogonal vector differential focusing array detector and proposed a detection signal processing method for this detector. In result, they achieved a lifting height of 2-3 times the pipeline diameter. Although the harmonic magnetic field detection method is suitable for the detection of defects in steel pipelines with large lift-offs, the current signal extraction methods are complex and the detection results have a high false alarm rate, which limits its practical application in engineering. Therefore, it is necessary to develop a high signal-to-noise ratio detection probe to quickly and accurately detect pipeline defects and locate them.

Non-Destructive Testing (NDT) methods based on the electromagnetic induction theory [9] usually suffer from the excitation magnetic field signal interference with the detection signal. Chady *et al.* [14] designed a probe that generated a zero flux axis, which consisted of a ferrite core and four magnetic pillars arranged 90°apart around the core, with the core wound in the receiving coil and the pillars wound in the excitation coil. As a result. they were able to obtain the image of a 3 mm crack at a lifting height of 1.25 mm. Liu *et al.* [15] designed an eddy current sensor array consisting of a periodic excitation coil and multiple differential detection coils, which increased the defect detection resolution by 1000 times. Hayashi *et al.* [16] designed a differential probe with two sets of *tunnel magnetoresistance* (TMR) sensors, which could effectively suppress interference signals by using the differential method. Trung [17] designed a uniform eddy current converging excitation coil and differential coil receiving probe with which minor defects were successfully detected at a lifting height of 0.25 mm. Xu *et al.* [18] proposed a system for differential eddy current detection which utilized the basic principle of alternating current bridge. By analysing the voltage difference between the two coils in the bridge circuit without lifting off, they obtained the signal amplitude and phase changes caused by a 0.2 mm crack. Moreover, Pasadas *et al.* [19] designed an eddy current probe with dual excitation coils and a sensing coil They successfully used it to conduct detection experiments on defects with a diameter of 2 mm at a lifting height of 0.5 mm. Although much progress has been made in the detection of steel pipelines without removing cladding, the existing probes still have a low lifting height (usually within 10 mm) and there is also the problem of coupling interference between the excitation magnetic field signal and the induction magnetic field signal, which have a significant negative impact on detection accuracy.

To address the issues above, in this work, we propose a differential compensation probe to remove the interference of excitation magnetic field signals to significantly improve the accuracy of the harmonic magnetic field detection method. We present the working principle of the proposed probe and detection system. The feasibility of the proposed probe is analysed and verified using a finite element model. The preparation method and hardware circuit design of the probe are described in detail. The experimental setup for detecting defects in steel pipelines with a cladding layer was constructed, and the experiments and analysis were carried out to verify the feasibility and effectiveness of the method. The consistent results of the theoretical analysis, numerical simulation, and experimental testing indicate that the differential compensation probe has the advantages of simple structure, large lifting distance, and high detection accuracy. It is expected that the differential compensation probe will promote the application of harmonic magnetic field detection methods in engineering practice, including pressure pipelines and vessels with cladding layers.

Metrol. Meas. Syst., Vol. 32 (2025), No. 1, pp. 1–21
DOI: 10.24425/mms.2025.152775

2. Probe principle and structural design

2.1. Harmonic magnetic field detection principle

Harmonic magnetic field detection is an electromagnetic non-destructive detection method consisting of a low-frequency carrier wave and high-frequency multiple harmonics. Fig. 1 is a schematic diagram of a typical harmonic excitation source signal and its composition simulated in MATLAB. The red signal represents the harmonic detection signal, and the magenta and blue signals are low-frequency carrier signals and high-frequency multiple harmonics, respectively. The low-frequency carrier signals [13] effectively overcome the skin effect, enhancing the penetration capability of the detection signal. However, excessively low excitation frequencies make it challenging to balance detection speed and signal resolution for long-distance pipelines. Therefore, a detection signal frequency of 25 Hz was selected.

High-frequency harmonic detection signals exhibit high sensitivity [21] and are particularly effective at detecting small defects. However, the selection of high-frequency harmonic signals is influenced by the inductive reactance of the excitation coil and the rated output power of the harmonic excitation source. Consequently, the high-frequency harmonics include the fundamental frequency at 300 Hz, as well as the third and fifth harmonics [13]. Therefore, the harmonic detection signal $f(t)$ is a periodic signal generated by the superposition of several sinusoidal signals of different frequencies, and its mathematical model can be expressed as follows:

$$f(t) = A_0 \sin(2\pi f_0 t + \theta_0) + \sum_{i=1}^{n} A_i \sin(2\pi f_i t + \theta_i), \tag{1}$$

where: A_0, f_0 and θ_0 are the amplitude, frequency, and starting phase of the low-frequency carrier sinusoidal signal. A_i, θ_i and f_i are the amplitude, frequency, and starting phase of the high-frequency sinusoidal signal, respectively.

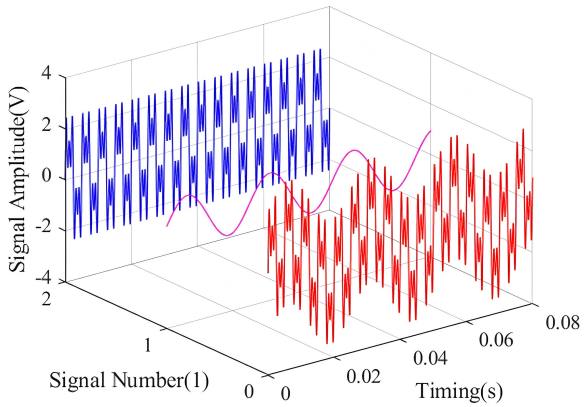

Fig. 1. Harmonic excitation source signal.

The schematic diagram of the detection system is shown in Fig. 2. The coil of the detection probe is connected to a harmonic current by the harmonic excitation power supply, and the excitation coil generates a harmonic magnetic field. The excitation magnetic field passes through the air and the cladding layer to reach the steel pipeline. The steel pipeline is excited by the excitation magnetic field and generates induced eddy currents, which produce an magnetic field

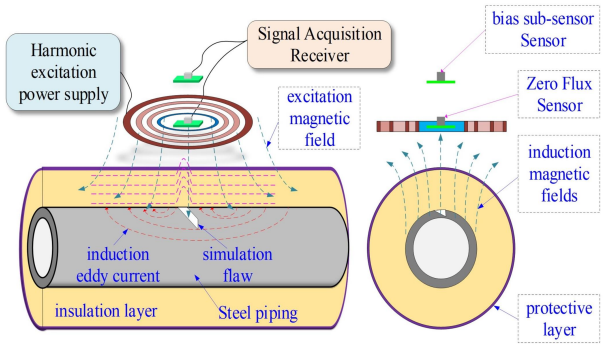

Fig. 2. Schematic diagram of the detection system.

that contains information about the detection region. Upon reaching the region of pipeline damage, the induced eddy currents are affected by a change in the electric conductivity of the pipeline due to a variation in the relative cross-section. At this time, the magnetic field signals are acquired by triaxial TMR sensors [22, 23], and the magnetic field signals are captured and stored by the data acquisition device.

2.2. Probe operation principle

Reducing the interference of the excitation magnetic field signal is the key method to realise the extraction of the detection signal of the pipeline without removing the cladding layer. The direction, magnitude, and propagation distance of the magnetic field generated by the coil are closely related to the winding direction, current direction, radius, and number of turns of the coil. An ideal zero flux point can be achieved at a point in space by adjusting the coil parameters. Based on the considerations above, four coaxial coils are arranged in the same plane, as shown in Fig. 3a. The brown coil is the excitation coil, which serves to provide the main excitation magnetic field for the detection. The orange coil and the yellow coil are Magnetic Focusing Coil 1 and Magnetic Focusing Coil 2, respectively, which serve to compensate for the excitation coil and provide the magnetic field focusing. The blue coil is the dephasing coil, which is designed

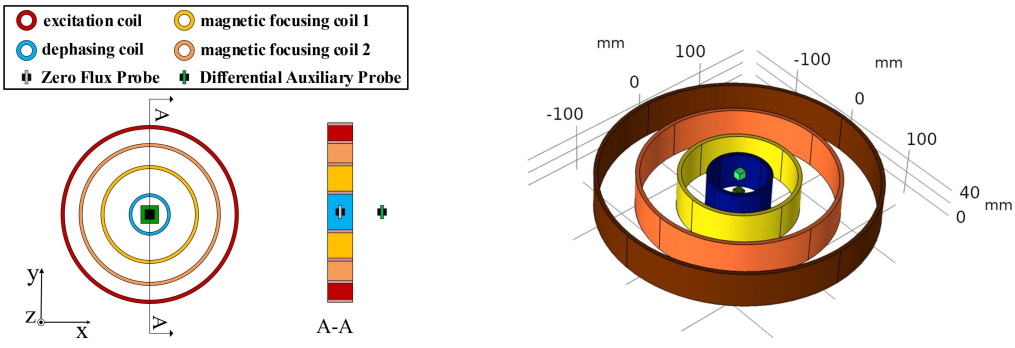

(a) (b)

Fig. 3. Detection probe for removing the excitation field.

to generate a magnetic field in the opposite direction of the excitation as well as the magnetic focusing coil to realize the purpose of generating a zero flux point on the axis of the coil. The middle purple is the location of the zero flux probe, which is in the centre of the coil. The zero magnetic flux sensor searches for zero flux points on the coil axis through the helical vice. The light green probe arranged on the upper side of the probe axis is the differential auxiliary probe of the three-axis magnetic field sensor which is used to collect the pure excitation magnetic field signals. Subsequently, the signal differentiation with the zero flux probe signal will be performed.

According to the Biot-Savart law and the formula for calculating the magnetic field component of a single-turn coil at any point in space [24], the magnetic field strength of a single-turn coil at a certain point in space is described as follows:

$$\begin{cases} \boldsymbol{B_x} = \dfrac{\mu_0 I R}{4\pi} \displaystyle\int_0^{2\pi} \dfrac{z\cos\beta \boldsymbol{i}}{\left(R^2 + y^2 + z^2 - 2yR\sin\beta\right)^{\frac{3}{2}}} d\beta \\ \boldsymbol{B_y} = \dfrac{\mu_0 I R}{4\pi} \displaystyle\int_0^{2\pi} \dfrac{z\sin\beta \boldsymbol{j}}{\left(R^2 + y^2 + z^2 - 2yR\sin\beta\right)^{\frac{3}{2}}} d\beta \\ \boldsymbol{B_z} = \dfrac{\mu_0 I R}{4\pi} \displaystyle\int_0^{2\pi} \dfrac{(R - x\cos\beta - y\sin\beta)\boldsymbol{k}}{\left(R^2 + y^2 + z^2 - 2yR\sin\beta\right)^{\frac{3}{2}}} d\beta \end{cases}, \tag{2}$$

where β is the pole angle in polar coordinates, μ_0 is the vacuum permeability, I is the energizing current, and R is the coil radius. According to (2), when the magnetic sensor is arranged at the centre of the axis, the magnetic field components in the x-axis and y-axis direction are 0. The excitation coil and two magnetic focusing coils are used to ensure that the excitation of the pipeline with cladding is achieved at a large lifting height. Therefore, the ideal zero-flux point can be found by cancelling the magnetic field component in the z-axis direction using an offsetting excitation magnetic field coil. As shown in Fig. 2, the magnetic field at the coil axis (0, 0, z) can be described as follows:

$$\begin{cases} \boldsymbol{B_x} = 0 \\ \boldsymbol{B_y} = 0 \\ \boldsymbol{B_z} = \dfrac{\mu_0 \boldsymbol{I k}}{2} \left[\dfrac{N_1 R_1^2}{\left(R_1^2 + z^2\right)^{\frac{3}{2}}} + \dfrac{N_2 R_2^2}{\left(R_2^2 + z^2\right)^{\frac{3}{2}}} + \dfrac{N_3 R_3^2}{\left(R_3^2 + z^2\right)^{\frac{3}{2}}} - \dfrac{N_4 R_4^2}{\left(R_4^2 + z^2\right)^{\frac{3}{2}}} \right] \end{cases} \tag{3}$$

where N_1, N_2, N_3, and N_4 represent the number of turns of the excitation coil, Magnetic Focusing Coil 1, Magnetic Focusing Coil 2, and the coil that counteracts the excitation magnetic field, respectively. R_1, R_2, R_3, and R_4 represent the radius of the excitation coil, Magnetic Focusing Coil 1, Magnetic Focusing Coil 2, and the coil that counteracts the excitation magnetic field, respectively. The triaxial magnetic field strength at the centre point (0,0,0) can be described as follows:

$$\begin{cases} \boldsymbol{B_{x0}} = 0 \\ \boldsymbol{B_{y0}} = 0 \\ \boldsymbol{B_{z0}} = \dfrac{\mu_0 \boldsymbol{I k}}{2} \left[\dfrac{N_1}{R_1} + \dfrac{N_2}{R_2} + \dfrac{N_3}{R_3} - \dfrac{N_4}{R_4} \right] \end{cases}, \tag{4}$$

According to (3), by fixing the radius and turns of the excitation coil, Magnetic Focusing Coil 1, Magnetic Focusing Coil 2, it is possible to calculate the N_4 and R_4 of the coil that counteracts the

excitation magnetic field This process facilitates the convergence of $\boldsymbol{B_{z0}}$ towards zero. To solve the problem of the residual excitation magnetic field signal in the actual design process, the method of collecting pure excitation magnetic field and zero magnetic field signal and making a difference is applied to further remove the residual excitation magnetic field signal. By selecting a point in space (0, 0, z_1), the magnetic field intensity $\boldsymbol{B_{z1}}$ of this point is obtained, and the ratio α of the magnetic field intensity at two points can be expressed as follows:

$$\alpha = \frac{\boldsymbol{B_{z1}}}{\boldsymbol{B_{z0}}}. \tag{5}$$

The magnetic field detected in the space is a combination of an excitation magnetic field, an induced magnetic field generated by pipelines, and other magnetic fields. The strength of the spatial magnetic field ($\boldsymbol{B_{sum}}$) is described as follows:

$$\boldsymbol{B_{sum}} = \boldsymbol{B_m} + \boldsymbol{B_s} + \boldsymbol{B_{other}} \tag{6}$$

where $\boldsymbol{B_m}$ is the magnetic field generated by the probe coil, $\boldsymbol{B_s}$ is the secondary magnetic field generated by the excited magnetic field of the pipeline, and $\boldsymbol{B_{other}}$ is the magnetic field generated by other factors. According to the propagation characteristics of the magnetic field, the zero flux sensor is close to detecting the object, and the secondary magnetic field in the z-axis direction at the zero magnetic flux point ($\boldsymbol{B_{s\_z0}}$) is much larger than the secondary magnetic field in the z-axis direction at the compensation difference point ($\boldsymbol{B_{s\_z1}}$). Therefore, with the magnetic field strength in the z-axis direction at the zero flux point ($\boldsymbol{B_{sum\_z0}}$) minus the magnetic field strength in the z-axis direction at the compensation point ($\boldsymbol{B_{sum\_z1}}$), the probe acquisition magnetic field strength ($\boldsymbol{\Delta B_z}$) can be described as follows:

$$\boldsymbol{\Delta B_z} = \boldsymbol{B_{sum\_z0}} - \frac{\boldsymbol{B_{sum\_z1}}}{\boldsymbol{\alpha}} \approx \boldsymbol{B_{s\_z0}} - \frac{\boldsymbol{B_{s\_z1}}}{\boldsymbol{\alpha}} \approx \boldsymbol{B_{s\_z0}}. \tag{7}$$

Similarly, for the x-axis and y-axis, differential compensation processing is also required due to the position error of the sensor assembly.

3. Finite Element Analysis of the Principles and Performance of Detection Probes

3.1. Probe model construction and magnetic field simulation analysis

3.1.1. Probe model

Here, we use the AC/DC module of COMSOL Multiphysics finite element simulation software for coil theoretical design. As shown in Fig. 3b, a three-dimensional (3D) model of the detection probe is established which consists of four coils, two TMR magnetic sensors (domain probes instead), and an air domain. Regarding the coils, the excitation coil is set to have a radius of 175 mm with 100 turns, Magnetic Focusing Coil 1 a radius of 125 mm with 100 turns, Magnetic Focusing Coil 2 a radius of 75 mm with 100 turns, and the coil that counteracted the excitation magnetic field a radius of 40 mm with 109 turns, all coils are placed in an air domain with a side length of 1000 mm. We select copper for the coil and air for the air domain from the built-in material library. Next, we set the number of coil turns, coil type, current direction, and coil excitation in the model, and connected the four coils in series. By analysing the skin effect of the pipeline and the reflection coefficient of the electromagnetic wave, the characteristic frequency of the detection signal is selected to ensure the effective propagation distance and sufficient energy intensity of the detection

signal [13]. The circuit interface provides a superposition of four sinusoidal current sources with a current of 5 A and frequencies of 25 Hz, 300 Hz, 900 Hz, and 1.5 kHz. The harmonic magnetic field detection is based on Maxwell's electromagnetic field theory.

3.1.2. Finite element simulation of removing excitation magnetic fields

According to (2), it can be seen that the x-direction and y-direction magnetic field strength components on the axis of the probe coil model are zero. Therefore, using or not using the blue coil in Fig. 3a is applied to verify its effect on removing the interference of the excitation magnetic field signal, and the simulation results are shown in Fig. 4. Fig. 4a and 4b are the magnetic field with and without the blue coil, respectively. The results show that when the blue coil is installed at the centre of the coil (0, 0), the magnetic field strength is significantly smaller and the magnetic flux density arrows at the point away from the centre of the coil remain almost unchanged. For the case without the blue coil, as shown in Fig. 4b, the magnetic field strength at the centre of the coil (0, 0) is very high. Next, we analyse the variation rule of magnetic flux intensity on the coil axis and plot the results in Fig. 4c. It can be found that there is a zero flux point in the magnetic field when using the blue coil to remove the excitation magnetic field. As the distance from the centre of the coil increases, the magnitude of the magnetic field strength produced by the two sets of

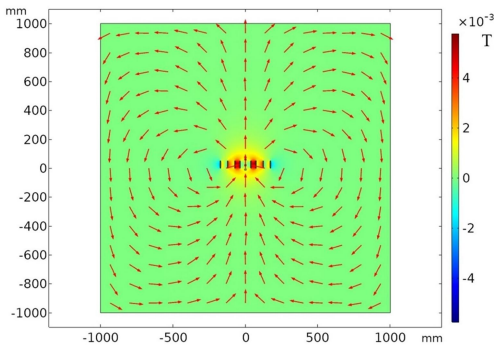

(a) Magnetic field loop with the blue coil

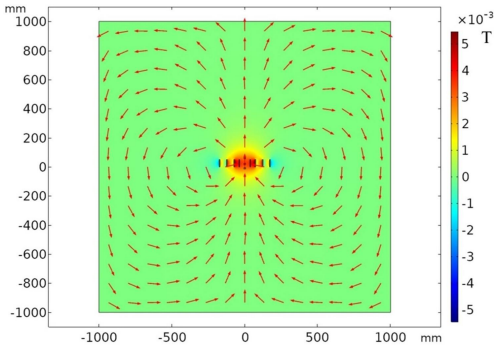

(b) Magnetic field loop without the blue coil

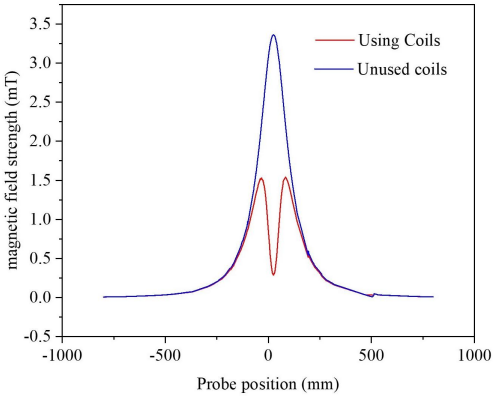

(c) Z-axis magnetic field strength (B_z)

Fig. 4. Simulation results of removing the primary magnetic field.

simulation experiments gradually overlaps. Therefore, the results show that using the blue coil to remove the excitation magnetic field not only provides a zero flux point for the detection probe but also ensures that the excitation coil works well within the detection range.

3.2. Simulation analysis of the probe

3.2.1. Probe application simulation

We establish a simulation model for defect detection in pipelines with a cladding layer, and it is shown in Fig. 5. Based on removing the excitation magnetic field simulation modelling, steel pipe was added to the model.

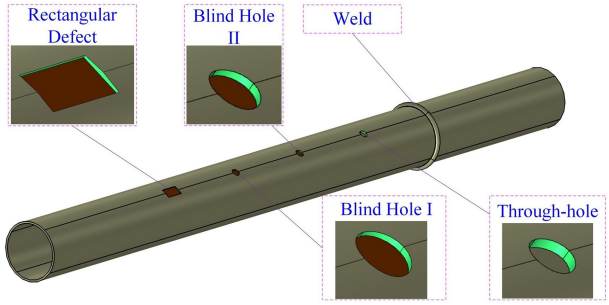

Fig. 5. Diagram of the simulation model.

The geometric parameters of the pipe are set to a diameter of 300 mm, a wall thickness of 10 mm, and a length of 4000 mm, and steel was selected as the pipeline material . The geometrical parameters of the cladding are set to a thickness of 200 mm, an inner diameter of 300 mm, and a length, of 4000 mm. The geometric parameters of the air domain are set to a length of 5000 mm, a width of 3000 mm, and a height of 2000 m. The axial direction of the pipeline is set to the x-axis, the circumferential direction is set to the y-axis, and the radial direction is set to the z-axis. The detection probe is arranged above the steel pipeline and close to the cladding. Harmonic excitation currents are introduced through COMSOL's circuit interface which is connected to the excitation coil. To avoid edge effects, the starting and stopping positions of the detection probe are kept 500 mm away from the end of the pipe. The detection probe moves along the x direction for defect detection. The detection probe sequentially scans rectangular metal defects, blind hole defects at different depths, and through holes in steel pipelines. The parameters of the defects are shown in Table 1.

Table 1. Defect parameters.

	Rectangular defects	Blind hole I	Blind hole II	Through-hole
Area (mm^2)	2000	200π	200π	200π
Depth (mm)	2	4	6	8

3.2.2. Simulation Results

As shown in Fig. 6, the simulation results of pipeline defect detection show significant changes in the magnetic field strength in the x- and z-directions. The most pronounced change in the simulated signal for the pipeline weld is due to a larger defect area resulting in a larger change in

the induced eddy currents in the pipeline, and thus a larger change in the induced magnetic field. The simulated signals of the through-hole defect and blind-hole defects show that the conforming magnetic field signal amplitude is affected by the defect depth. The depth of the defect causes changes in induced eddy currents, which in turn leads to changes in the induced magnetic field. The signal changes of weld seams and large areas of missing metal are more pronounced than blind-hole and through-hole defects. The detection effect of the y-direction is relatively poor, and it is analysed that the circumferential magnetic field of the pipeline is weak, and the damage signal needs to be further extracted by combining the algorithm. In addition, the simulation analysis results guide experimental testing.

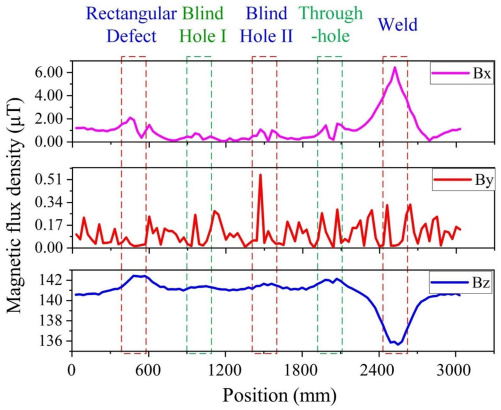

Fig. 6. Simulation results.

4. Detection Probe Fabrication

4.1. Detection Probe Processing

As shown in Fig. 7, the probe is composed of four coaxial detection coils and two TMR magnetic sensors. The detection coils are made up of copper enamelled wire and acrylic tubing, and the size and number of turns of the detection coils are kept consistent with the simulation model. Four detection coils are connected in series to ensure that the excitation field is in the same phase. The excitation coil, Magnetic Focusing Coil 1, and Magnetic Focusing Coil 2 are

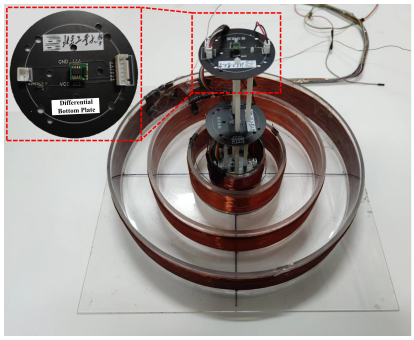

Fig. 7. Physical image of the detection probe and the differential compensation PCB base.

wound with a left-hand direction enamelled wire. The coil that counteracts the excitation magnetic field is wound with a right-hand direction enamelled wire, to achieve the goal of generating a zero flux point at the axis of the coil. The probe receiving section is composed of two TMR magnetic sensors, a *printed circuit board* (PCB) base, nylon nut studs, an acrylic bracket set, and a height-adjustable nut. The surface of the zero flux PCB base is equipped with a zero flux TMR magnetic sensor, and the bottom of the zero flux PCB base is fixed with an acrylic plastic bracket. The acrylic plastic bracket is glued to the height adjustment nut which is connected to the probe base plate height adjustment stud. By rotating the nut, the sensor can locate the zero magnetic flux point on the axis of the detection coil. The bottom of the differential compensation PCB base is fixed to the zero magnetic flux point PCB base surface with nylon nut bolts, and the surface of the differential compensation PCB base is equipped with a compensating TMR magnetic sensor.

The capacitance and inductance of a coil are frequency-dependent, they can be described as follows:

$$X_L = 2\pi f L, \tag{8}$$

$$X_C = \frac{1}{2\pi f C}, \tag{9}$$

where X_L is the probe loop inductive reactance, X_C is the compensating capacitive reactance and f is the excitation frequency. The specific method of calculation is given elsewhere [25].

An impedance analyser was used to analyse the impedance of the series-connected detector coils. The characteristic curves of frequency versus impedance and phase were obtained and plotted in Fig. 8. The characteristic curve shows that the detection coil operates within 50.365 kHz. According to (2), the excitation magnetic field strength is positively correlated with the magnitude of the excitation current. The magnitude of the excitation current is the ratio of the voltage of the excited power supply to the impedance of the detection coil, and can described as:

$$Z = \sqrt{R + (X_L - X_C)^2}, \tag{10}$$

where R is the loop resistance value. One can substitute the inductive reactance values of the coil at different eigenfrequencies in the harmonic signal into (10) to determine the demanded capacitance value. The high-frequency harmonic excitation currents cause large inductive reactance in the detection coil, which makes the amplitude of the excitation current at different frequencies inconsistent with the simulated current. Therefore, balancing the impedance of different frequencies

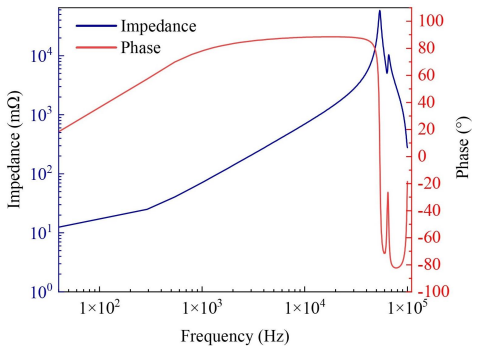

Fig. 8. Characteristic curves of probe coil impedance and phase.

Metrol. Meas. Syst., Vol. 32 (2025), No. 1, pp. 1–21
DOI: 10.24425/mms.2025.152775

in the loop is achieved by connecting a capacitor in series with the detection coil loop. The resistance of the detection coil was measured by a multimeter to be 10.961 Ω. The impedance of the detection coil at the frequencies of 25 Hz, 300 Hz, 900 Hz, and 1.5 kHz in the characteristic curve was selected, and the mean value of the coil inductance was found to be 13.7 mH by combining (8), (9) and (10).

4.2. Differential compensation

The position accuracy of the zero-flux sensor is limited by using the helical pair, which leads to a strong residual excitation field signal in the output signal of the zero-flux sensor. To solve the problem of the residual excitation signal, the compensated magnetic field sensor and zero-flux magnetic field sensor are arranged in an asymmetric structure, and the residual excitation signal is removed with the differential method, as shown in (7).

A differential compensation amplifier circuit is designed for realising the differential compensation of the two signals, which consists of a zero flux magnetic field sensor signal preprocessing circuit, a compensation magnetic field sensor preprocessing circuit, a high pass filter circuit, a reverse phase circuit, and a post differential gain circuit as shown in Fig. 9.

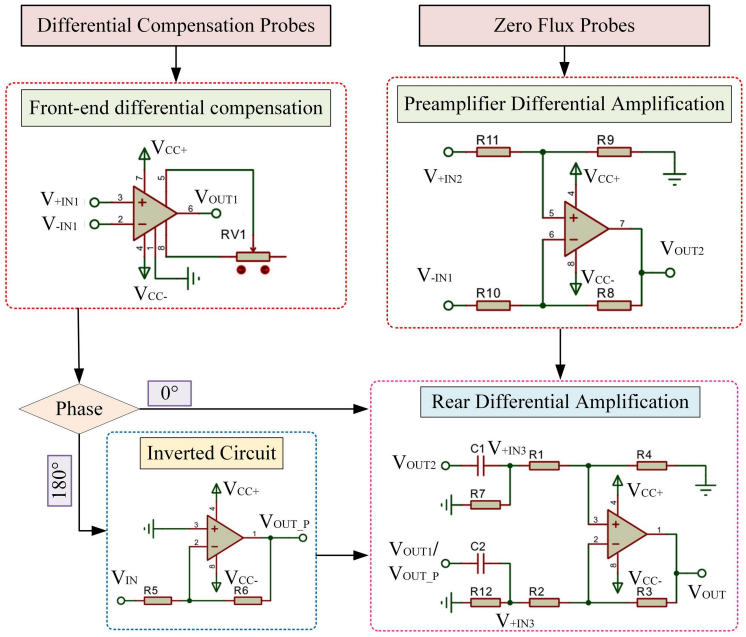

Fig. 9. Schematic diagram of the differential compensation amplifier circuit.

Since the output signal of TMR2309m is a differential signal, differential preprocessing of the detection signal is required. This paper utilizes an AD8279 operational amplifier to process the output signal of the zero-flux sensor, which uses a built-in resistor for twice-the-gain differential amplification operation. The formula for the differential amplification output signal amplitude is as follows:

$$V_{\mathrm{OUT}} = 2 \times (V_{+\mathrm{IN}} - V_{-\mathrm{IN}}) \tag{11}$$

where V_{+IN1} and V_{-IN1} are the input zero flux sensor single-axis differential signals, respectively. V_{OUT} for the differential is two times the output zero flux sensor signal voltage. For the differential compensation preamplifier circuit, we use an AD8421 operational amplifier with a variable resistor (R_{G1}) connected in series to the two R_G pins of the amplifier . The differential compensation output signal amplitude can be described as follows:

$$V_{OUT} = \left(1 + \frac{R_1}{R_{G1}}\right) \times (V_{+IN} - V_{-IN}) + V_{REF} \tag{12}$$

where V_{+IN2} and V_{-IN2} are the input differential compensation sensor single-axis differential signals, V_{OUT} is the differential compensation sensor signal voltage output after the differential, R_1 is the operational amplifier AD8421 internal fixed value and equals 9.9 KΩ. R_{G1} is a variable resistor resistance, the value of R_{G1} is determined according to the amplitude of the signal output from the zero-flux preamplification circuit. V_{REF} is the reference voltage and equals 0V. Since the output voltage of this circuit is (1+ R_1/R_G) times the sensor differential voltage, the output voltage of the zero-flux preamplification circuit is subjected to two-stage gain to provide a margin for compensation matching. The reverse amplification circuit consists of an operational amplifier LM358 and two 10 KΩ resistors. Input signal amplitude inversion can be performed to achieve matching of x and y-axis signal output directions between the two sensors. The RC high pass filtering circuit can achieve a cut-off frequency of 11.3 Hz filtering while removing DC signals and low-frequency interference signals in the circuit. The differential compensation post-amplification circuit is composed of the same elements as the differential compensation pre-amplification circuit, consisting of an operational amplifier AD8421 and a variable resistor (RG2). The input signals V_{+IN3} and V_{-IN3} are the signals of the corresponding axes of the two sensors' output processed by the high pass filter. The amplification factor is controlled by the variable resistor RG2, which can achieve a final circuit output of ±10 V.

5. Experiments

5.1. Experimental Setup

The experimental setup includes a harmonic excitation source, a high-speed acquisition card, a detection probe, a positioning device, a steel pipeline, and a pipeline cladding, as shown in Fig. 10. The output signal amplitude of the harmonic excitation power supply is 60V. The high-speed acquisition card has a single channel of 18 kHz, and it can display and store the acquired data. During the experiment, the probe was arranged directly above the cladding layer and scanned slowly along the axis of the pipeline. After data collection, based on the principle of phase-locked amplification [26, 27], we use MATLAB to process the stored experimental data and further analyse the amplitude changes of defect signals.

Combining simulation results with factors such as the skin effect, comprehensive experiments were conducted to detect extensive metal loss on the surface of the pipeline and welds. A D300 mm #45 steel pipe was selected to carry out the pipeline defect detection experiment for different thickness cladding, as shown in Fig. 11a. The cladding layer was formed by stacking multiple cladding layers with a single layer thickness of 9 cm, as shown in Fig. 11b, and there were gaps between the layers of the cladding layer for easy installation on the pipeline. To simulate long-distance pipeline detection without removing the cladding layer, during the experiment, the probe was driven to move along the top of the pipeline by pushing the short cladding layer. The weld seam was formed by welding two pipe sections with a width of about 1.5 cm, as shown in

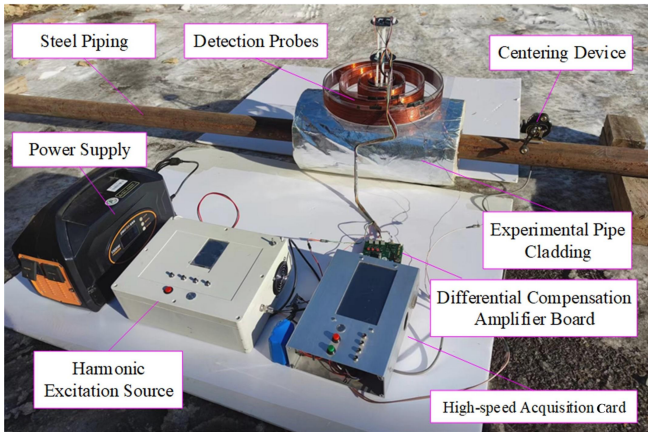

Fig. 10. Experimental setup.

Fig. 11c. Different areas of metal thinning with a depth of about 1.5 mm were used as experimental metal defects. The size of Metal Defect I was 5 cm × 5 cm, as shown in Fig. 11d. The size of Metal Defect II is 10 cm × 10 cm, as shown in Fig. 11e. For the working conditions above, cladding layers of 9 cm and 18 cm thickness were used for the experiments, respectively.

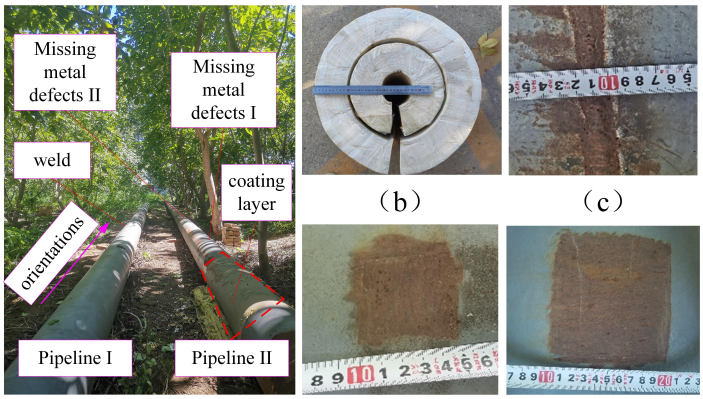

Fig. 11. Pipeline and defects in the experiment.

5.2. Experimental results

As shown in Fig. 12, the defect detection experiment is carried out on two steel pipelines, the start position and end position of pipeline detection are selected to be more than 500 mm away from the end of the pipeline, respectively, which is used to avoid the edge effect interfering with the detection signal [28]. The previous simulation results have shown that the magnetic field signal at the weld seam changed the most significantly. We first conduct weld seam detection on the pipeline based on the differential compensation probe. We place the probe directly above Pipeline 1 for weld seam detection, with the starting and ending positions located 2000 mm on both sides of the weld seam, and the thickness of the cladding layer is 27 cm. The weld seam detection is

carried out along Region I, and the probe moves at a distance of 4000 mm. Secondly, we conduct defect detection for type I Missing Metal in Pipeline 2, with defects located at the centre points of Region II. The amplitude of the damage signal is small. There are two types of thicknesses for the cladding layer: 9 cm and 18 cm. The probe moves at a distance of 2000 mm along Region II. Finally, the defect detection for Type II Missing Metal in Region III was conducted, and the defects are located at the centre points of Region III, and its length is 2000 mm. There are also two sizes of cladding thickness: 9 cm and 18 cm. Due to the differential compensation amplification circuit board achieving preliminary band-pass filtering of the detection signal, the phase-lock amplifier is directly used to process the detected signal. 25 Hz, 300 Hz, 900 Hz, and 1.5 kHz are selected as the reference signal frequencies respectively, and the amplitudes of the four demodulation signals are superimposed.

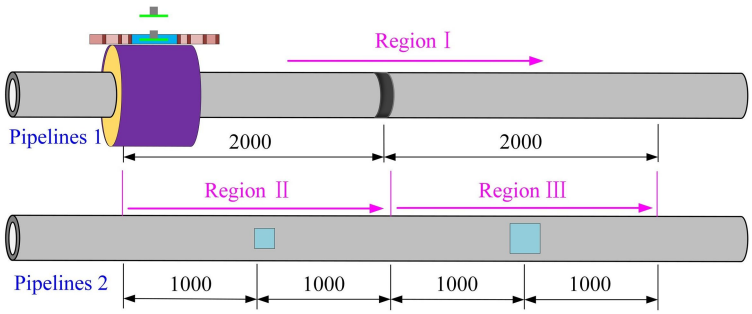

Fig. 12. Schematic diagram of the location of pipeline defects.

Figure 13 shows the experimental results of weld seam detection for Pipeline 1 with a cladding layer thickness of 27 cm. As shown in Fig. 13, the red-dashed box area corresponds to the position of the weld seam, and it can be observed that there is a significant change in the magnetic field intensity signal at the pipeline weld seam when the lifting distance is 27 cm. In the principle of the harmonic magnetic field detection method, the induced eddy current passing through the weld causes a change in the conduction path, resulting in a change in the amplitude of the induced magnetic field, which in turn, is reflected in the amplitude change of the magnetic field detection signal collected by the sensor. As the propagation range of the magnetic field increases with the lifting distance [29], the width of the obtained signal change is much larger than the actual weld width.

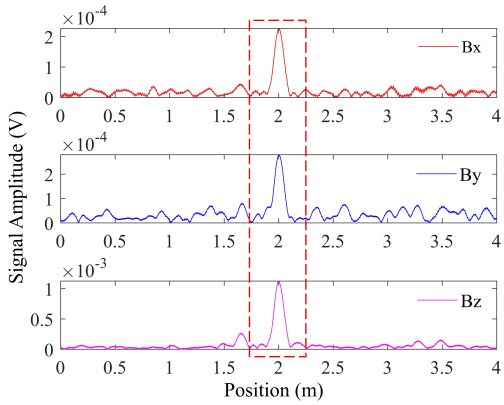

Fig. 13. Experimental results of weld seam detection for Pipeline I with a cladding layer thickness of 27 cm.

To further verify the effectiveness of the differential compensation probe in detecting defects in pipelines without removing the cladding layer, we conducted defect detection on Missing Metal I in Pipeline 2, and the detection results are shown in Fig. 14. In Fig. 14a, it can be seen that with the cladding layer thickness of 9 cm, the amplitude of the three-axis magnetic field intensity signal of the sensor shows significant changes at the defect location. To analyse the impact of the distance between the inspection probe and the pipeline on defect detection results, we conducted tests on a pipeline with a cladding thickness of 18 cm under identical experimental conditions, and the results are shown in Fig. 14b. Compared with the situation where the cladding layer thickness was 9 cm in Fig. 14a, the detection signal amplitude decreased under the coating layer thickness of 18 cm. However, combined with the signal changes of the sensor's three axes, the Missing Metal I can be located. From Fig. 14, it can be seen that as the thickness of the cladding layer increases, the detection sensitivity decreases. However, with the coating layer thickness of 18 cm, the defect information of the pipeline can still be detected. The detection signal of the x and y axis turned out to be a false alarm signal at 0.2 m, which was caused by the unsteady motion of the probe combined with the analysis of the experimental process.

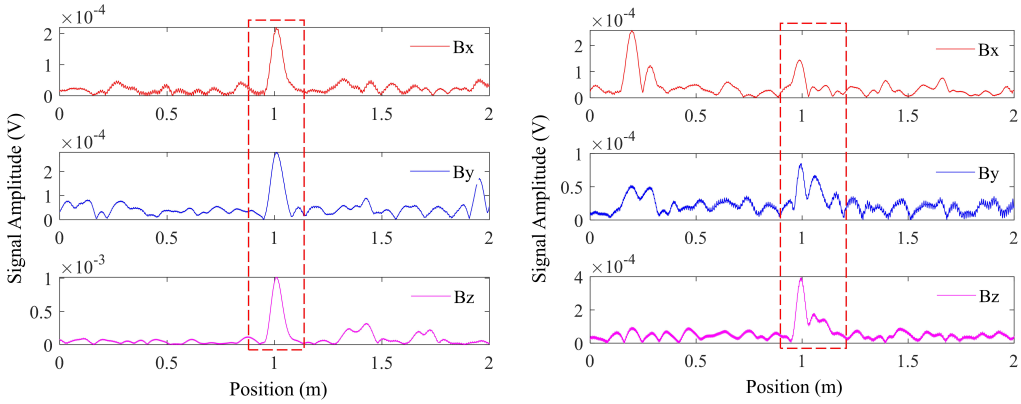

(a) 9 cm-thick cladding layer (b) 18 cm-thick cladding layer

Fig. 14. Detection results of Missing Metal I in Pipeline 2.

In addition, the Missing Metal II of Pipeline 2 shown in Fig. 12 was detected, and the results are shown in Fig. 15. From the detection results, it can be seen that there are two peaks in the magnetic field intensity signal of the defect area, which is caused by the wider actual size of Missing Metal II. As shown in Fig. 15a, with the cladding layer thickness of 9 cm, the amplitude of the three-axis signal of the sensor shows significant changes at the defect location. The signal-to-noise ratio of the x-axis signal decreases relative to the y-axis and z-axis because the induced current field formed on the pipeline surface has a larger impact range on the x-axis. As shown in Fig. 15b, with the cladding layer thickness of 18 cm, there is a significant change in the detection of Missing Metal II signal at the defect positions on the y-axis and z-axis, and the distance between the two peak values of the signal increases. Similar to Fig. 15a, the signal-to-noise ratio of the x-axis signal has decreased. As the lift increases, the change in defect position signal in the x-axis can be inferred from the y-axis and z-axis signals.

To further verify the ability of the detection probe to detect circumferential defects in pipelines, as shown in Fig. 16, it is arranged along the circumferential direction at different positions in Pipeline 2 to conduct detection experiments on Missing Metal I at different angles. During the detection process, the detection probe is placed on the pipeline cladding. Within the cross-section

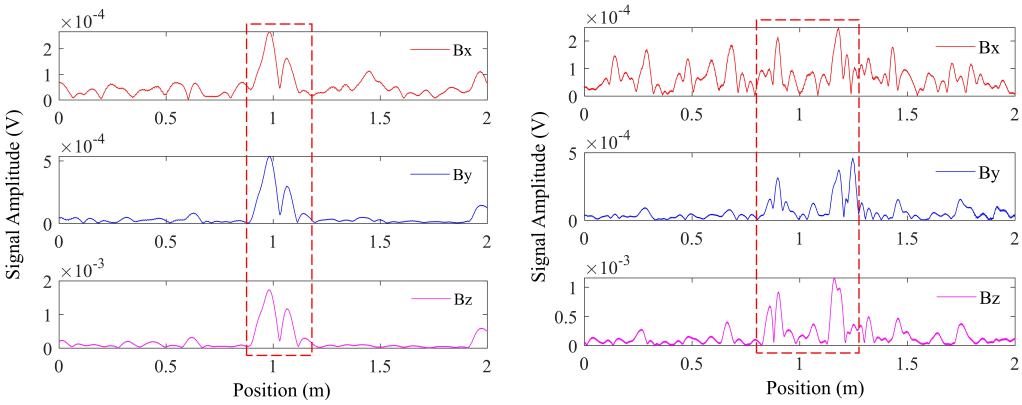

(a) 9 cm thick cladding layer (b) 18 cm thick cladding layer

Fig. 15. Missing Metal II detection results for Pipeline 2.

of the pipeline where the defect centre is located, it is assumed that the line connecting the defect centre and the pipeline centre is the defect orientation line, and the line connecting the probe and the pipeline centre is the detection orientation line. As shown in Fig. 16, the angles between the detection orientation line and the defect orientation line are 22.5°, 45°, 67.5° and 90°, respectively. The experimental steps are the same as the Missing Metal I detection steps for Pipeline 2 with a cladding layer thickness of 18 cm.

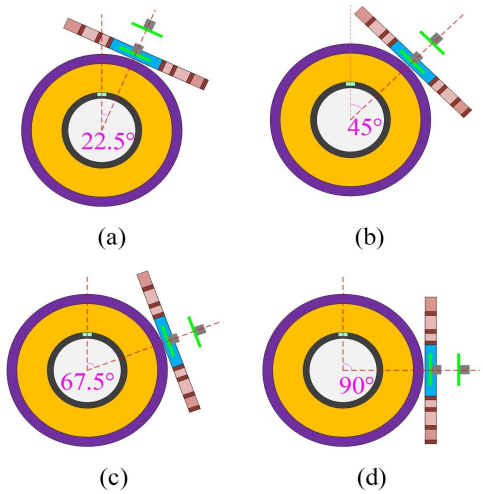

Fig. 16. Schematic diagram of the probe arrangement.

Figure 17 shows the defect detection results when the detection probes are distributed in the circumferential direction of the pipeline. With the weakening of the pipeline damage signal, the detection signal in the single-axis direction easily has alarm signals, and the detection signal analysis is carried out with the method of multi-axial signal comparison. When the angle between the detection orientation line and the defect orientation line is 22.5° and 45°, the detection results of the *y*-axis and z-axis can accurately locate the missing metal defect. Despite interference signals

caused by probe jitter, the detection results of the x-axis can still locate defects. When the angle is 67.5°, due to the increase in angle, the detection results of the x and z axes are affected by interference signals. However, the detection results of the y-axis can locate the position of the missing metal. When the angle continues to increase to 90°, it is difficult to locate metal defects in all three axial detection results. The experimental results indicate that the induced eddy currents are more concentrated below the detection probe, and the available detection area is approximately within ±60° between the detection orientation line and the defect orientation line.

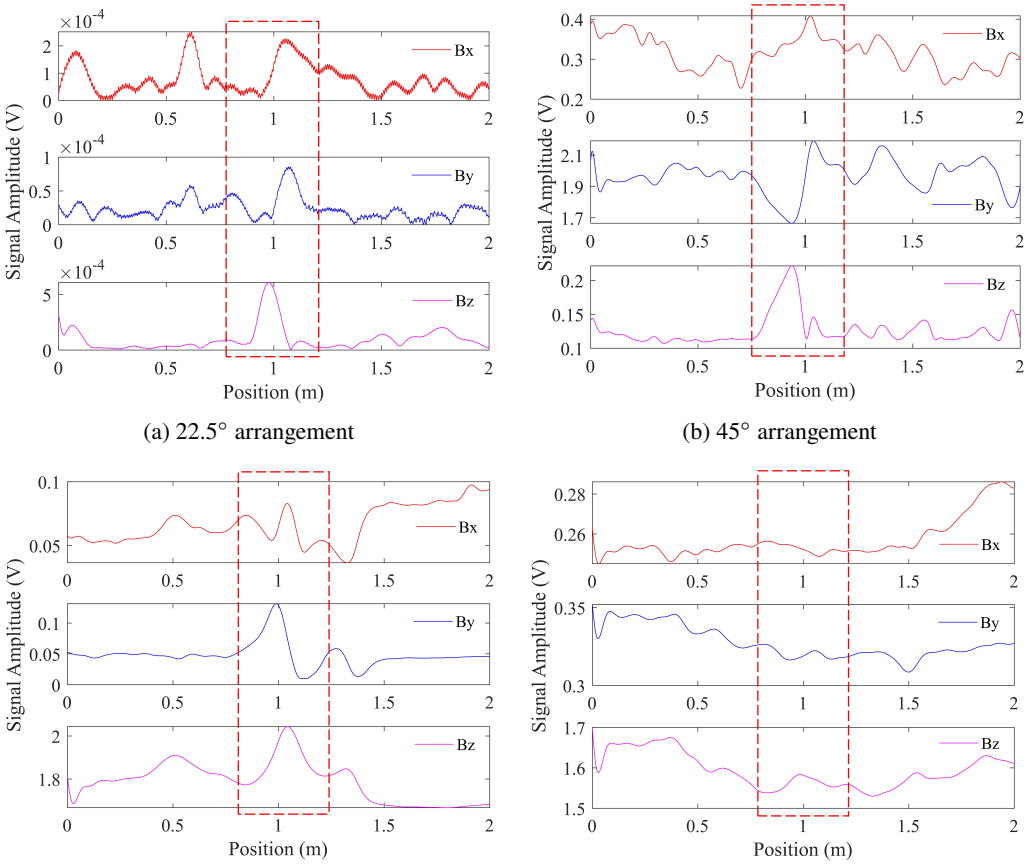

(a) 22.5° arrangement

(b) 45° arrangement

(c) 67.5° arrangement

(d) 90° arrangement

Fig. 17. Pipeline defect detection results under inclined angle conditions.

6. Conclusion

In conclusion, this work proposes a differential compensation probe for detecting steel pipelines without removing the cladding layer. The structural design of the differential compensation sensor is implemented, and the detection probe is composed of an excitation coil, a magnetic focusing coil group, a counter-excitation magnetic field coil, and two TMR magnetic sensors. The excitation coil and magnetic focusing coil generate and enhance the harmonic magnetic field used to excite

steel pipes, and the coil that counteracts the excitation magnetic field at the centre point of the excitation coil facilitates the collection of induced magnetic field signals by TMR magnetic sensors. The TMR magnetic sensor signals are arranged in a biased manner to further eliminate the excitation magnetic field. The working principle of the probe was analysed using finite element simulation, and the feasibility of using a differential distribution probe was verified. At the same time, we set up a pipeline detection experimental platform to verify the effectiveness of differential compensation probes in detecting defects in steel pipelines without removing the cladding layer. The experimental results show that the detection probe proposed in this work is very sensitive to the characteristics of pipeline defects. It can effectively remove the excitation magnetic field signal from the detection signal, avoiding magnetic saturation in TMR magnetic sensors. In addition, the combination of differential amplification compensation circuit further removes the interference of coupled excitation magnetic field and environmental magnetic field. The harmonic magnetic field detection method based on a differential compensation probe provides a new approach for defect detection in pipelines without removing the coating layer. It has broad application prospects in the detection of pressure pipelines and pressure vessels with cladding layers.

Acknowledgements

This work is supported by Beijing Municipal Science & Technology Commission, the Administrative Committee of the Zhongguancun Science Park grant No. Z231100006023011, and the R&D Program of Beijing Municipal Education Commission (KM202210005032).

References

[1] Wang, X., Yang, L., Sun, T., Rasool, G., Sun, M., Hu, N., & Guo, Z. (2023). A review of development and application of out-of-pipe detection technology without removing cladding. *Measurement*, *219*, 113249. https://doi.org/10.1016/j.measurement.2023.113249

[2] Wang, R., Kang, Y., Tang, J., Feng, B., & Deng, Y. (2020). A Novel Magnetic Flux Leakage Testing Method Based on AC and DC Composite Magnetization. *Journal of Nondestructive Evaluation*, *39*(4). https://doi.org/10.1007/s10921-020-00730-0

[3] Hutchins, D.A., Watson, R.L., Davis, L.A.J., Akanji, L., Billson, D.R., Burrascano, P., Laureti, S., & Ricci, M. (2020). Ultrasonic Propagation in Highly Attenuating Insulation Materials. *Sensors*, *20*(8), 2285. https://doi.org/10.3390/s20082285

[4] Ona, D.I., Tian, G.Y., Sutthaweekul, R., & Naqvi, S.M. (2019). Design and optimisation of mutual inductance based pulsed eddy current probe. *Measurement*, *144*, 402–409. https://doi.org/10.1016/j.measurement.2019.04.091

[5] Song, Y., & Wu, X. (2022). An analytical solution for vertical coils near a multi-layered metallic pipe in Pulsed Eddy Current Testing. *NDT & E International*, *125*, 102570. https://doi.org/10.1016/j.ndteint.2021.102570

[6] Abdul-Majid, S., & Balamesh, A. (2014). Single Side Imaging of Corrosion Under Insulation Using Single Photon Gamma Backscattering. *Research in Nondestructive Evaluation*, *25*(3), 172–185. https://doi.org/10.1080/09349847.2013.869376

[7] Oh, S., Cheong, Y., Kim, D., & Kim, K. (2019). On-Line Monitoring of Pipe Wall Thinning by a High Temperature Ultrasonic Waveguide System at the Flow Accelerated Corrosion Proof Facility. *Sensors*, *19*(8), 1762. https://doi.org/10.3390/s19081762

[8] Zaini, M.A.H.P., Saari, M.M., Nadzri, N.A., Aziz, Z., Ramlan, N.H., & Tsukada, K. (2021). Extraction of Flux Leakage and Eddy Current Signals Induced by Submillimeter Backside Slits on Carbon Steel Plate Using a Low-Field AMR Differential Magnetic Probe. *IEEE Access*, *9*, 146755–146770. https://doi.org/10.1109/access.2021.3123421

[9] Rifai, D., Abdalla, A., Ali, K., & Razali, R. (2016). Giant Magnetoresistance Sensors: A Review on Structures and Non-Destructive Eddy Current Testing Applications. *Sensors*, *16*(3), 298. https://doi.org/10.3390/s16030298

[10] Zhao, Y., Wang, X., Sun, T., Chen, Y., Yang, L., Zhang, T., & Ju, H. (2021). Non-contact harmonic magnetic field detection for parallel steel pipeline localization and defects recognition. *Measurement*, *180*, 109534. https://doi.org/10.1016/j.measurement.2021.109534

[11] Yuan, X., Li, W., Chen, G., Yin, X., Jiang, W., Zhao, J., & Ge, J. (2019). Inspection of both inner and outer cracks in aluminum tubes using double frequency circumferential current field testing method. *Mechanical Systems and Signal Processing*, *127*, 16–34. https://doi.org/10.1016/j.ymssp.2019.02.054

[12] Wang, X., Gu, Y., Chen, Y., Ullah, Z., & Zhao, Y. (2020). Research on a damage identification method of harmonic magnetic field detection in steel pipes with cladding. *Insight - Non-Destructive Testing and Condition Monitoring*, *62*(9), 533–539. https://doi.org/10.1784/insi.2020.62.9.533

[13] Zhao, Y., Wang, X., Chen, Y., Ju, H., Zhang, T., & Ullah, Z. (2019). Defect Detection of Metal Pipeline Based on Harmonic Eddy Current. *2019 Photonics &; Electromagnetics Research Symposium - Spring (PIERS-Spring)*, 700–704. https://doi.org/10.1109/piers-spring46901.2019.9017755

[14] Chady, T., & Sikora, R. (2003). Optimization of eddy-current sensor for multifrequency systems. *IEEE Transactions on Magnetics*, *39*(3), 1313–1316. https://doi.org/10.1109/tmag.2003.810412

[15] Liu, L., Chen, D., Pan, M., Tian, W., Wang, W., & Yu, Y. (2019). Planar Eddy Current Sensor Array with Null-Offset. *IEEE Sensors Journal*, *19*(12), 4647–4651. https://doi.org/10.1109/jsen.2019.2901351

[16] Hayashi, M., Saito, T., Nakamura, Y., Sakai, K., Kiwa, T., Tanikura, I., & Tsukada, K. (2019). Extraction Method of Crack Signal for Inspection of Complicated Steel Structures Using a Dual-Channel Magnetic Sensor. *Sensors*, *19*(13), 3001. https://doi.org/10.3390/s19133001

[17] Trung, L.Q., Kasai, N., Sekino, K., & Miyazaki, S. (2023). Eddy current convergence probes with self-differential and self-nulling characteristics for detecting cracks in conductive materials. *Sensors and Actuators A: Physical*, *349*, 114084. https://doi.org/10.1016/j.sna.2022.114084

[18] Peng, X.U., Chenlu, Z., Zhongxing, X.U., Ping, W. (2018). Rail crack identification method based on differential eddy current testing. *Nondestructive Testing*, *12*(40) 7-11, https://doi.org/10.11973/wsjc201812002

[19] Pasadas, D.J., Ramos, H.G., Baskaran, P., & Ribeiro, A.L. (2020). ECT in composite materials using double excitation coils and resonant excitation/sensing circuits. *Measurement*, *161*, 107859. https://doi.org/10.1016/j.measurement.2020.107859

[20] Wang, J., Yusa, N., Pan, H., Takagi, T., & Hashizume, H. (2013). Evaluation of Sensitivity of Remote Field Eddy Current Testing and Low-Frequency Eddy Current Testing for Inspecting Grooves of Metal Plate. *Materials Transactions*, *54*(1), 90–95. https://doi.org/10.2320/matertrans.m2012323

[21] Xu, P., Zeng, H., Qian, T., & Liu, L. (2022). Research on defect detection of high-speed rail based on multi-frequency excitation composite electromagnetic method. *Measurement*, *187*, 110351. https://doi.org/10.1016/j.measurement.2021.110351

[22] Fan, X., He, Y., Chen, T., & Hou, C. (2022). Research on crack monitoring technology of flexible eddy current array sensor based on TMR sensors. *Measurement*, *192*, 110926. https://doi.org/10.1016/j.measurement.2022.110926

[23] Betta, G., Ferrigno, L., Laracca, M., Rasile, A., & Sangiovanni, S. (2021). A novel TMR based triaxial eddy current test probe for any orientation crack detection. *Measurement*, *181*, 109617. https://doi.org/10.1016/j.measurement.2021.109617

[24] Wang, X., Gu, Y., Chen, Y., Ullah, Z., Pan, Q., & Zhao, Y. (2020). A new technology for steel pipeline damage detecting without removing cladding. *Measurement*, *159*, 107700. https://doi.org/10.1016/j.measurement.2020.107700

[25] Yu, S., Wei, Y., Zhang, J., & Wang, S. (2019). Noise Optimization Design of Frequency-Domain Air-Core Sensor Based on Capacitor Tuning Technology. *Sensors*, *20*(1), 194. https://doi.org/10.3390/s20010194

[26] Kishore, K., & Akbar, S.A. (2020). Evolution of Lock-In Amplifier as Portable Sensor Interface Platform: A Review. *IEEE Sensors Journal*, *20*(18), 10345–10354. https://doi.org/10.1109/jsen.2020.2993309

[27] Macias-Bobadilla, G., Rodríguez-Reséndiz, J., Mota-Valtierra, G., Soto-Zarazúa, G., Méndez-Loyola, M., & Garduño-Aparicio, M. (2016). Dual-Phase Lock-In Amplifier Based on FPGA for Low-Frequencies Experiments. *Sensors*, *16*(3), 379. https://doi.org/10.3390/s16030379

[28] Yang, L., Wang, X., Sun, T., Meng, T., Yang, X., Li, L., & Qi, Y. (2022). A technology of full perimeter inspection for steel pipeline without removing cladding. *Measurement*, *190*, 110746. https://doi.org/10.1016/j.measurement.2022.110746

[29] Qin, Y., Chen, J., Li, K., Zhang, W., Wang, W., Ouyang, J., & Yang, X. (2022). Eddy Current Magnetic Localization of Nonmagnetic Metal Targets Based on Metal Shell Model. *IEEE Sensors Journal*, *22*(11), 10774–10782. https://doi.org/10.1109/jsen.2022.3168612

Xinhua Wang received the B.Sc. degree from in 1992, the M.Sc. degree from the China University of Petroleum (East China) in 1997, and the Ph.D. degree from China University of Petroleum (Beijing) in 2000. Since 2000, he has been with the Faculty of Materials and Manufacturing, Beijing University of Technology. He is currently a professor and Ph.D. supervisor at Beijing University of Technology. His main research interests include pipeline NDT technologies and safety evaluation, pipeline corrosion and protection.

Zisheng Guo received the B.Sc. and M.Sc. degrees in mechanical engineering from Beijing Information Science and Technology University, China, in 2018 and 2022, respectively. He is currently pursuing the Ph.D. degree in pipeline NDT technologies and instruments from the Beijing University of Technology, Beijing, China. His research interests include the development of inspection instruments and harmonic nondestructive testing methods.

Naixiang Hu obtained a Bachelor's degree in mechanical engineering from the Shandong University of Science and Technology in 2021 and a Master's degree in mechanical engineering from the Beijing University of Technology in 2024. Currently, he works at the Beijing Chengjian Zhikong Technology Co., Ltd. as an embedded device developer and sensor application designer. His research interests include the development of detection instruments and nondestructive testing methods.

Peng Gao received the B.Sc. and M.Sc. degrees from Beijing Information Science and Technology University (BISTU) in 2009 and his Ph.D. degree from the Beijing Institute of Technology (BIT) in 2014. He has been working as a lecturer at the School of Materials and Manufacturing, of the same university since 2020. His main research interests are the phonon scattering characteristics and defect detection methods for traversing pipelines.

Lin Yang received the B.Sc. degree and the M.Sc. degrees in mechanical and electronic engineering from the Shandong University of Technology, Zibo, China, in 2016 and 2019, respectively. He is currently pursuing the Ph.D. degree in pipeline NDT technologies and instruments from the Beijing University of Technology, China. His research interests include the development of detection instruments and EM detection methods.

Ghulam Rasool received his Ph.D. degree from Zhejiang University in 2022. He has been working at the School of Materials and Manufacturing, Beijing University of Technology since 2022. He is currently a postdoctoral fellow at the Beijing Institute of Technology. His main research interest is fluid mechanics.

Tao Sun received the B.Sc. degree from China Agricultural University in 2009, and the Ph.D. degree from Peking University in 2014. Since 2020, he has been with the Faculty of Materials and Manufacturing, Beijing University of Technology. He is currently an associate professor at Beijing University of Technology. His main research interest is phonon scattering characteristics and inspection method of defects for crossing pipelines.

Yongsheng Qi received the B.Sc. degree and the M.Sc. degree in mechanical and electronic engineering from the Shandong University of Technology, Zibo, China, in 2016 and 2020, respectively. He is currently pursuing the Ph.D. degree from the Beijing University of Technology, China. His main research interests are nondestructive testing techniques based on elastic waves and acoustic signal processing.